Alkyl Ketene Dimer Grafted Cationic Cellulose Stabilizing Nano Magnesium Oxide for Efficient Protection of Aging Paper

Bei He
South China University of Technology
Jingbo Ai
South China University of Technology
Junli Ren (renjunli@scut.edu.cn)
South China University of Technology https://orcid.org/0000-0002-7837-8252
Lihong Zhao
South China University of Technology
He Zhao
South China University of Technology
Chuanfu Liu
South China University of Technology
Huiming Fan
South China University of Technology

Research Article

Keywords: Cellulose, Amphiphilic modification, Dispersion, Aging paper

Posted Date: February 28th, 2022

DOI: https://doi.org/10.21203/rs.3.rs-1347521/v1

Abstract

Alkyl ketene dimer grafted cationic cellulose (AKD-g-CMCC) was designed to stabilize nano magnesium oxide (MgO) in low polarity mixed solution of hexamethyldisiloxane (HMDO) and isopropanol (IPA) for protection of aging paper. The highly stable nano MgO organic colloid exhibited a small average particle size (200 nm) and low viscosity (2.26 mPa·s), which is beneficial for the efficient protection of aging paper. Evaluation results showed that properties of treated aging paper were improved. Small-size MgO (200 nm) uniformly deposited on the paper endowed the treated paper with mild pH (8.30) and sufficient alkali reserve (1.00%, calcium carbonate equivalent) for deacidification. Meanwhile, the tensile index and tear index of treated paper increased by 40.78% and 27.28%, respectively. Moreover, the treated paper presented the low chromatic aberration (ΔE=0.46) and the negligible influence in the appearance and clarity of writing. Additionally, the treated paper also had the excellent anti-aging and anti-adhesion performance.

1. Introduction

Hundreds of millions of paper materials are suffering from the serious aging and degradation over the world (Cappitelli et al. 2010; Liu and Wang 2010; Wilson 2012; Norris and Gutierrez 2017). The acid-catalyzed hydrolysis of paper fibers is the central reason for the damage of aging paper due to the accumulation of acidic substances. Cleavage of 1,4-β-glycosidic bond of cellulose caused the reduce of the degree of polymerization (*DP*), further resulting in the weak mechanical strength of aging paper, which is unfavorable for their conversation and utilization (Carter 1996a; Baty et al. 2010; Area and Ceradame 2011; Zervos and Alexopoulou 2015). Moreover, oxidation of cellulose is another critical factor for the degradation of aging paper. The chromophores were generated from paper fibers by the promotion of ultraviolet light, high alkalinity or oxidizing substances, causing paper discoloration, especially paper containing lignin (Carter 1996b; Conte et al. 2012). Therefore, deacidification, enhancement and anti-oxidation are the indispensable procedures for the protection of aging paper.

Currently, deacidification methods were mainly developed based on the principle of acid-base neutralization that alkaline agents neutralize acidic substances to inhibit acid-catalyzed hydrolysis of paper fibers and improve the durability of aging paper. Most of deacidification agents can be summarized as alkaline aqueous solutions, alkaline organic colloids, and alkaline gases (Baty et al. 2010; Zervos et al. 2015). Alkaline aqueous solutions are environment-friendly and low-cost, regrettably, the treated aging paper needs a time-consuming drying process and is easy to be crumpled and low-mechanical-strength (Baglioni et al. 2014). Additionally, alkaline gases such as ammonia, diethyl zinc (DEZ) and dry ammonia ethylene oxide (DAE) can easily achieve mass deacidification, but the low alkali reserves and serious safety hazards limit their application (Cheradame et al. 2003). Mass deacidification methods mainly developing from alkaline organic colloids have been widely applied in libraries and archives, including Wei T'o process, Bookkeeper process, and Papersaver process®, etc., which are preferred by conservators for their excellent deacidification effect, simple and efficient process, and small negative impact on the appearance and writing clarity of aging paper based on the rapid volatilization of

low-polar organic solvents such as dichlorodifluoromethane, perfluoroheptane, and hexamethyldisiloxane (HMDO) (Potthast and Ahn 2017; Hubbe et al. 2017; Hubbe et al. 2018). However, these mass deacidification methods did not significantly improve the mechanical performance of treated aging paper, especially for the fragile aging paper.

Enhancement of aging paper has also been studied based on the chemical or physical methods. Synthetic polymers (silicone resin (Ferrandin-Schoffel et al. 2020), acrylic resin (Xu et al. 2020), epoxy resin (Pereira-Pardo and Korenberg 2018), polyurethane (Isca et al. 2016; Isca et al. 2019), etc.) and natural polymers (cellulose (Santos et al. 2015; Li et al. 2019; Xu et al. 2020), chitosan (Jiang et al. 2016; Jia et al. 2020), starch (Lama et al. 2020), etc.) were used to reinforce aging paper. In comparison, cellulose is preferred for its good compatibility with paper fibers and excellent reinforcement performance. However, the poor solubility of cellulose in water or general organic solvents causes the restriction on its applications (Li et al. 2019). Chemical modification of cellulose is the common method to improve its solubility or dispersibility (Xu et al. 2020). Nevertheless, most of the reinforcement materials based on cellulose derivatives for the protection of aging paper were mainly dissolved or dispersed in water, which was inefficient due to the time-consuming drying process (Santos et al. 2015; Li et al. 2019; Palladino et al. 2020). Treatment with aqueous solutions may also cause some adverse effects on appearance of aging paper, such as wrinkles and water stains (Baty et al. 2010; Baglioni et al. 2014; Zervos et al. 2015).

Accordingly, it may be a better idea to dissolve or disperse cellulose derivatives in low-polar organic solvent for efficient and non-destructive protection of aging paper (Giorgi et al. 2010; Baglioni et al. 2014). Amornkitbamrung et al. (2015; 2018; 2020) repeatedly reported that the hydrophobic trimethylsilylcellulose could be dissolved in HMDO to disperse magnesium hydroxide ($Mg(OH)_2$) nanoparticles for deacidification and enhancement of aging paper. The treated paper presented a good deacidification and enhancement effect. However, the low dispersion stability and the high hydrophobicity of treated paper may be not beneficial to the long-term preservation of aging paper (Jeong et al. 2014). In contrast, amphiphilic polymer may be a better choice for the stable dispersion of inorganic nanoparticles in low-polar organic solvents because it could stably disperse in low-polar organic solvents by self-assembly (Narouz et al. 2017; Yi et al. 2020).

In this work, a new kind of amphiphilic cellulose polymers were designed and prepared by for stabilizing nano MgO in the low polarity mixed solvent of HMDO and isopropanol (IPA), which would be applied for mass deacidification and enhancement of aging paper. The amphiphilic cellulose polymers (AKD-g-CMCC) were prepared by grafting 2,3-epoxypropyltrimethylammonium chloride (ETA) and alkyl ketene dimer (AKD) onto microcrystalline cellulose (MCC). The chemical structure was characterized in detail. Then, the transmittance, particle size distribution and viscosity were also used to prove the dispersion performance of the nano MgO organic colloid. The relationship between chemical structure of AKD-g-CMCC and dispersion properties was clearly explained. In this contribution, this highly stable nano MgO organic colloid would simultaneously impart ageing paper with the deacidification, enhancement and anti-aging performance.

2. Experimental Section

2.1. Reagents and materials

MCC (α-cellulose, 25μm), sodium hydroxide (NaOH, AR), AKD (purity, 90%), ETA (purity, 95%), HMDO (AR), IPA (AR), dichloromethane (CH_2Cl_2, AR), and nano MgO (50nm) were purchased from Shanghai Macklin Biochemical Co., Ltd. Copper (II) ethylenediamine was obtained from China National Pulp and Paper Research Institute. All reagents were used as received without further purification. The aging paper samples got from an aged book published in 1980 (pH = 4.70).

2.2. Preparation of AKD-g-CMCC

Three kinds of AKD-g-CMCC polymers were prepared by ETA and AKD grafted onto MCC. The preparation of AKD-g-CMCC were shown in Fig. 1. The chemical structures and reaction process were shown in Fig. S1. CMCC was firstly synthesized by ETA grafting onto MCC. Briefly, 8.0 g of MCC was added to 100 mL of NaOH aqueous solution (14 wt.%) and kept stirring for 1 hour. Then the alkalized cellulose was centrifuged and washed with deionized water to neutrality and then dried under vacuum at 50 ℃ for 12 hours. Soon afterwards, the alkalized cellulose was added into 200 mL of mixed solution (IPA/NaOH aqueous solution (1.0 mol/L) = 8:2, v/v) and reacted with ETA (n(anhydroglucose unit (AGU)):n(ETA) = 1:3) at 75 ℃ for 4 hours. IPA can effectively inhibit the hydrolysis of CMCC during the reaction process (Odabas et al. 2016; Odabas et al. 2017; He et al. 2019). The synthetic product was filtrated and washed with IPA and deionized water, and then dried under vacuum at 50 ℃ for 12 hours to obtain CMCC (*DS* = 0.283). Subsequently, AKD-g-CMCC was prepared by AKD grafting onto CMCC. In detail, the molted AKD was evenly dissolved in HMDO by stirring at 75°C. Then the synthetic CMCC was added into HMDO based on n(AKD): n(AGU) = 1:1, 2:1 and 3:1. And the mixture was sheared at 2000 r/min for 10 minutes and reacted at 105°C for 20 minutes. Finally, the prepared product was washed and filtrated with CH_2Cl_2, and dried under vacuum at 60 ℃ for 12 hours to obtain the pure AKD-g-CMCC polymers. Based on the *DS*, the products were named as $CMCC_{0.283}$, $AKD_{0.009}$-g-$CMCC_{0.277}$, $AKD_{0.027}$-g-$CMCC_{0.253}$, and $AKD_{0.024}$-g-$CMCC_{0.223}$, respectively.

2.3. Preparation of Nano MgO Organic Colloid

The schematic diagram of nano MgO organic colloid preparation was also shown in Fig. 1. Firstly, 0.1 ~ 0.7 wt.% of AKD-g-CMCC was added to 500 mL mixed solution of HMDO and IPA (5:5, v/v) and dissolved by 20 KHz ultrasound treatment at 80% power (SCIENTZ-IID, Xinzhi, China) for 5 min. And then 2.0 g/L of nano MgO was added and dispersed by ultrasound treatment at same conditions for 5 min again. The obtained nano MgO organic colloid was denoted as xAKD_n-g-$CMCC_m$/MgO /HMDO/IPA (5:5), where x represents the addition amount of AKD-g-CMCC, n means the *DS* of AKD, and m means the *DS* of ETA. For comparative analysis, the controls (xAKD_n-g-$CMCC_m$/HMDO, xAKD_n-g-$CMCC_m$/HMDO/IPA (5:5), 2g/L MgO/HMDO/IPA (5:5)) were also prepared under the same conditions.

2.4. Treatment of paper samples

The aging paper samples were firstly placed in vacuum and dried at 50 ℃ for 12 h to control moisture in the range of 1–2%. The pre-dried paper samples were immersed in the highly stable nano MgO organic colloid of AKD-g-CMCC/MgO/HMDO/IPA (5:5) for 5 minutes. The treatment method was denoted as ACMMHI. In comparison, the untreated paper samples were also carried out under the same conditions (named as UT). The treated paper samples were air dried in a fume hood for 30 minutes and then placed in vacuum at 50 ℃ to dry for 12 hours again. Then the treated paper samples were subjected to the damp heat aging box at T = 80 ℃, RH = 65% for 3 days. Finally, these treated paper samples were placed in the constant temperature and humidity room for the moisture balance and test.

2.5. Characterization and measurements

2.5.1. GPC

The molecular weight (M_w) of AKD was detected by tetrahydrofuran phase gel chromatography (GPC, Agilent1100, America). 1.0 mg of AKD was dissolved in 1 mL of tetrahydrofuran. After the solution was filtered, 0.5 ml of the clear solution was taken for detection by GPC.

2.5.2. FT-IR and solid-state ^{13}C NMR

The samples were characterized by Fourier transform infrared spectrophotometer (FT-IR, VERTEX 33, Germany), solid-state ^{13}C nuclear magnetic resonance spectrometer (^{13}C NMR, AVANCE III HD 600, Germany, spinning speed = 5.000 ± 0.002 kHz). The *DS* of CMCC and AKD-g-CMCC were calculated according to the formula (1) and (2) respectively:

$DS = I_{CH3}/3I_{C1}$ (1)

$DS = I_{CH2}/47I_{C1}$ (2)

where I_{CH3} denotes the integral of resonance peak of CH_3 on the quaternary ammonium group of CMCC at 57 ppm; Ic_1 denotes the integral of resonance peak of C_1 of cellulose at 105 ppm; 3 is the number of -CH_3 on the quaternary ammonium group of CMCC; I_{CH2} denotes the integral of resonance peak of -CH_2- on the alkyl chain of AKD at 20 ~ 30 ppm; 47 is the number of -CH_2- unit on alkyl chain of AKD.

2.5.3. Intrinsic viscosities and relative molecular weight

The intrinsic viscosities ($[\eta]$) of samples was determined by the viscosity method according to ISO 5351/1 B. Then the relative molecular weight (M_r) was calculated according to the Mark-Houwaink formula: $[\eta] = K*M_r^{\alpha}$, where K is 0.13 and α is 0.905. Furthermore, the viscous degree of polymerization () of samples was calculated by the Mark-Houwink-Sakurada equation:= $(0.75[\eta])^{1/0.905}$ (Shinoda et al. 2012).

2.5.4. UV-visible spectrophotometer, DLS and viscosity

The transmittance value of nano-MgO organic colloid was measured by a UV-visible spectrophotometer (UV1900, Japan) in the range 200–900 nm with resolution of 0.5 nm. The stability of the dispersion system was analyzed through the change of transmittance value at λ = 600 nm. After standing for same time, the smaller change of transmittance indicates better stability of the dispersion system. The average particle size was determined by dynamic light scattering (DLS, SZ-100Z, Japan). The viscosity of nano-MgO organic colloid was measured with a digital viscometer (NDJ-5S, China).

2.5.5. SEM-EDS and AFM

The microscopic morphology and elemental mapping of samples were observed by a scanning electron microscope (SEM, SU5000, Japan) working at an accelerating voltage of 5.0 kV and 15 kV, respectively. Element mapping was also performed with an energy spectrum model Super-X energy dispersive spectrometer (EDS) detector. Atomic force microscopy (AFM, Multimode 8, Germany) was also used to analyze the morphology of samples working on a Bruker instrument dimension ICON controller equipped with silicon cantilever probe with the tapping mode. The photo of paper samples before and after treatment were obtained by the *HP* scanner (Scan Jet Pro 2500, China).

2.5.6. pH value and alkaline reserve

The pH value of the paper samples was measured by cold extraction according to ISO 6588-1:2021. Then alkaline reserve of treated paper sample was assessed according to ISO/TS 18344:2016.

2.5.7. Tensile index and tear index

Tensile strength of the paper samples was measured according to ISO 1924-2:2008 with instrument (L&W CE062, Sweden). Tensile index was calculated according to tensile strength and basis weight of paper. Tear index is the ratio of tearing resistance to the basis weight of the paper sample. Tearing resistance was measured according to ISO 4046-5:2016 with L&W tear tester (L&W 009, Sweden). All reported values were calculated as averages over ten replicates for each sample (Ma et al. 2021).

2.5.8. Chromatic coordinate

Chromatic coordinate (Δ*E*) was calculated based on the following Eq. (3) and the (*L, a, b*) values of paper samples were measured by L&W whiteness tester (Elrepho 070, Sweden) according to ISO 12625-7:2014.

$$\Delta E\,(L,\,a,\,b) = \sqrt{(\Delta a)^2 + (\Delta b)^2 + (\Delta L)^2} \qquad (3)$$

where Δ*L* is the lightness difference; Δ*a* is the red/green difference; and Δ*b* is the yellow/blue difference.

2.5.9. Static water contact angle

The static water contact angle (WCA) was measured according to ISO 15989:2004. The treated paper samples were tested by the surface WCA tester (OCA40 Micro, Germany).

3. Results And Discussion

3.1. Characterization of AKD-g-CMCC

To figure out the chemical structure of AKD-g-CMCC, the FT-IR patterns were firstly recorded. As shown in Fig. 2a, the spectra of MCC exhibited a series of characteristic absorption peaks of cellulose in the range from 4000 cm^{-1} to 500 cm^{-1}, such as the stretching vibration of O-H at 3440 cm^{-1}, C-H stretching vibration at 2890 cm^{-1}, O-H bending of absorbed moisture at 1640 cm^{-1}, C-O-C asymmetric stretching vibration at 1160 cm^{-1}, the in-plane ring stretching at 1108 cm^{-1}, and C-O stretching vibration at 1030 cm^{-1} (Schwanninger et al. 2004; Chung et al. 2004). Compared with MCC, the spectra of CMCC displayed a series of stronger C-O-C stretching vibration peaks at 1340 ~ 1020 cm^{-1} in Fig. 2b, which may be attributed to the formation of new ether groups on cellulose (Sirviö et al. 2011; Chaker and Boufi 2015). Furthermore, the spectra of CMCC exhibited two new absorption peaks corresponding to the asymmetric CH_3 at 1480 cm^{-1} and the C-N stretching vibration at 1420 cm^{-1}, implying that part of hydroxyl groups on cellulose were substituted by the quaternary ammonium groups after quaternization (Odabas et al. 2017; He et al. 2019).

In order to further verify the successful preparation of AKD-g-CMCC polymers, the chemical structure of AKD was analyzed in detail. Firstly, the M_w of AKD was detected by GPC. As depicted in Fig. S2, five response peaks appeared in the molecular weight distribution of AKD and the M_w of the largest response peak is 771, which indicated that AKD wax is mixture and the M_w of its main component is 771. Moreover, AKD contains a four-membered lactone ring with two long-chain alkyl structure ($C_4H_2O_2$-$(CH_2)_n(CH_3)_2$) (Fig. S1) (Yang et al. 2016; Tyagi et al. 2018). Basing on the chemical structure formula and M_w of AKD, therefore, the chemical formula of the main components of AKD could be confirmed as $C_4H_2O_2$-$(CH_2)_{47}(CH_3)_2$. Besides, as shown in the FT-IR pattern of AKD in Fig. 2, sharp peaks at 1720 cm^{-1} and 1850 cm^{-1} are related to C = C double bond and C = O double bond in carboxyl group of lactone ring, respectively. The peaks at 1470 cm^{-1} and 720 cm^{-1} are related to the bending mode of CH_2 bonds. Moreover, sharp peaks from 2848 cm^{-1} to 2918 cm^{-1} are because of C-H stretching vibrations (Esmaeili et al. 2020). Furthermore, as depicted in the FT-IR spectra of AKD-g-CMCC, the characteristic absorption peaks of β-ketone ester at 1710 cm^{-1} and 1750 cm^{-1} implied that lactone ring reacted with hydroxyl groups of cellulose. It could be also found that the spectra of AKD-g-CMCC exhibited the strong characteristic absorption peaks of C-H at 2918 cm^{-1}, 2848 cm^{-1}, 1470 cm^{-1} and 720 cm^{-1}, which further indicated that AKD successfully grafted onto CMCC. In addition, it was not observed the characteristic peaks of lactone ring of AKD at 1720 cm^{-1} and 1850 cm^{-1}, indicating that the unreacted AKD was removed from AKD-g-CMCC through CH_2Cl_2 washing. Therefore, the above analysis verified that AKD-g-CMCC was synthesized successfully (Song et al. 2012; Yan et al. 2016).

To further calculate the *DS* of CMCC and AKD-g-CMCC, the dry powders of AKD, MCC, CMCC, and AKD-g-CMCC were characterized by solid state ^{13}C-NMR. The corresponding integral of various types of C and

DS were listed in Table S1. The original analysis spectrums of solid state ^{13}C-NMR were shown in Fig. S3(a-f). As depicted in Fig. 3a, the typical resonance peaks of cellulose were presented at 107.41 ppm for C_1, 91.23 ppm for C_{4cryst}, 85.13 ppm for $C_{4amorph}$, 77.18 ppm for C_3 and C_2, 74.63 ppm for C_5, 67 ~ 62 ppm for C_6 (Liu et al., 2006; Harini, Ramya, & Sukumar, 2018). Compared with MCC, a new resonance signal of CMCC in Fig. 3b and AKD-g-CMCC in Fig. 3(c-e) appeared at 56.0 ppm corresponding to the methyl carbons (C_{10}) of the ETA substituents, which demonstrated that ETA was grafted onto MCC successfully (Li et al. 2016; Kono 2017). According to formula 1, the *DS* of ETA grafted onto CMCC and three kinds of AKD-g-CMCC polymers were calculated as 0.283, 0.277, 0.253, and 0.223, respectively. Furthermore, as shown in Fig. 3f, the chemical shifts at 171.7 ppm, 144.8 ppm, 104.6 ppm, 54.3 ppm are assigned to four types of C (C_a, C_c, C_d, and C_b) on lactone ring and the chemical shifts at 15 ppm, 25 ~ 35 ppm are assigned to CH_3 and CH_2 of AKD, respectively (Yan et al. 2016). Compared with the AKD, no chemical shifts of lactone ring appeared on the ^{13}C-NMR spectrum of AKD@CMCC in Fig. 3(c-e), further confirming that no unreacted AKD remained in AKD-g-CMCC. Moreover, the *DS* of AKD for three kinds of AKD-g-CMCC polymers were calculated by formula 2 as 0.009, 0.027, and 0.024, respectively.

3.2. Dispersion performance of nano MgO organic colloid

Based on above analysis, three kinds of AKD-g-CMCC polymers were used to disperse nano MgO in HMDO. As depicted in Fig. 4a, the nano MgO organic colloid of 0.5wt.% $AKD_{0.024}$-g-$CMCC_{0.223}$/MgO/HMDO/IPA (5:5) exhibited the smallest change of transmittance after standing for 12 and 24 hours, indicative of the most stable dispersion performance, which may be due to the greater steric hindrance of $AKD_{0.024}$-g-$CMCC_{0.223}$ in the mixed solution of HMDO and IPA. In fact, the steric hindrance of polymer is mainly related to its molecular weight (Jeon et al. 2019). According to the Mark-Houwaink formula: $[\eta] = K^* M_r^a$, the M_r of AKD-g-CMCC polymers was calculated and listed in Table S2. Obviously, compared with $AKD_{0.009}$-g-$CMCC_{0.277}$ (M_r = 1582.06) and $AKD_{0.027}$-g-$CMCC_{0.253}$ (M_r = 1943.61), $AKD_{0.024}$-g-$CMCC_{0.223}$ had the highest M_r (2021.34). This result was consistent with the dispersion stability of the three kinds of nano MgO organic colloids. Moreover, the steric hindrance of AKD-g-CMCC polymer is also related to the ratio of *DS* of grafted hydrophobic group and hydrophilic group (Ran et al. 2009; Shukla and Shahi 2018). As presented in Table S2, the ratio of *DS* of AKD to CMCC in $AKD_{0.024}$-g-$CMCC_{0.223}$ was also the highest, which mean that $AKD_{0.024}$-g-$CMCC_{0.223}$ with the high ratio of grafted hydrophobic group is beneficial to stabilize nano MgO in the low-polarity mixed solution of HMDO and IPA.

Moreover, the concentration of the $AKD_{0.024}$-g-$CMCC_{0.223}$ also significantly affected the dispersion stability of nano MgO organic colloid. As shown in Fig. 4b, with the concentration of the $AKD_{0.024}$-g-$CMCC_{0.223}$ increased, the dispersion stability of nano MgO organic colloid firstly increased and then decreased. When the concentration was 0.5 wt.%, this nano MgO organic colloid presented the smallest change of transmittance after standing for 24 hours, achieving the most stable dispersion, while the higher or lower concentration of $AKD_{0.024}$-g-$CMCC_{0.223}$ obviously decreased the dispersion stability, which may be due to the unsuitable steric hindrance. As reported by references (Yi et al. 2020; Wang et al. 2020),

high concentrations of surfactants in colloids could form the larger steric hindrance, preventing inorganic nanoparticles from entering the micelles. Instead, the smaller steric hindrance caused by low-concentration of surfactants could also not form the stable micelles. Therefore, in this work, the optimized concentration of the $AKD_{0.024}$-g-$CMCC_{0.223}$ in the nano MgO organic colloid is 0.5 wt.%.

Furthermore, IPA also played a crucial role in improving the dispersion stability of nano MgO organic colloid. As shown in Fig. 4c, IPA could improve the dispersion stability of $AKD_{0.024}$-g-$CMCC_{0.223}$ and nano MgO in HMDO and further promote the dispersion stability of nano MgO organic colloid, which was owning to the aggregation inhibition of $AKD_{0.024}$-g-$CMCC_{0.223}$ and nano MgO through interface regulation of IPA. The dispersion mechanism of IPA was proposed and clarified by experimental and computational studies, which will be reported in detail in another work. Briefly, IPA has one hydrophilic hydroxyl group and two hydrophobic methyl groups. IPA was easy to penetrate into $AKD_{0.024}$-g-$CMCC_{0.223}$ polymer and tended to form hydrogen bonds with its hydroxyl groups and quaternary ammonium groups for reducing its surface energy, which could prevent self-aggregation of $AKD_{0.024}$-g-$CMCC_{0.223}$ polymer in low-polarity HMDO. Additionally, the hydroxyl group of IPA could easily adsorb on the surface of MgO to prevent aggregation of nano MgO (Reynaert et al. 2006). More importantly, comparing with 2 g/L MgO/HMDO/IPA (5:5), adding 0.5 wt.% $AKD_{0.024}$-g-$CMCC_{0.223}$ further improved the dispersion stability of nano MgO organic colloid. Thus, the results indicated that IPA and $AKD_{0.024}$-g-$CMCC_{0.223}$ had a synergistic dispersion effect on nano MgO in HMDO.

In addition, the nano MgO organic colloid of 0.5wt.% $AKD_{0.024}$-g-$CMCC_{0.223}$/MgO/HMDO/IPA (5:5) also had smaller average particle size (200 nm) and more concentrated distribution as shown in Fig. 4d. This reason was attributed to the synergistic dispersion of $AKD_{0.024}$-g-$CMCC_{0.223}$ and IPA. In the absence of IPA, Fig. 4d presented the biggest and narrow particle size distribution (980 nm) of the dispersion system of 0.5wt.% $AKD_{0.024}$-g-$CMCC_{0.223}$/HMDO. As a comparison, adding IPA could markedly decrease the average particle size of $AKD_{0.024}$-g-$CMCC_{0.223}$ in HMDO (300 nm). Additionally, compared with the particle size distribution of 2 g/L MgO/HMDO/IPA (5:5), adding $AKD_{0.024}$-g-$CMCC_{0.223}$ could obviously improve the uniformity of particle size distribution of nano MgO organic colloid.

The above result could be supported by the SEM and AFM images. As shown in Fig. 5a, the SEM image of 0.5 wt.% $AKD_{0.024}$-g-$CMCC_{0.223}$/HMDO/IPA (5:5) presented that the micro-nano-scale flakes were deposited on the conductive adhesives. From the Fig. 5b, the SEM image of 0.5 wt.% $AKD_{0.024}$-g-$CMCC_{0.223}$/MgO/HMDO/IPA (5:5) showed that lots of nanoparticles deposited on the surface of micro-nano-scale flakes. The results further revealed the dispersion mechanism that the micro-nano-scale flakes of $AKD_{0.024}$-g-$CMCC_{0.223}$ improved the dispersion stability by loading with nano MgO prevented the agglomeration in the mixed solution of HMDO and IPA. Meanwhile, the AFM image (Fig. 5c) of 0.5 wt.% $AKD_{0.024}$-g-$CMCC_{0.223}$/MgO/HMDO/IPA (5:5) clearly presented the average particle size (about 200 nm) of the stable nano MgO organic colloid, which was consistent with the DLS's data in Fig. 4d. In addition,

Fig. S4 also exhibited the low viscosity (2.26 mPa·s) of nano MgO organic colloid, which indicated that the stable nano MgO organic colloid is beneficial for the batch processing of aging paper.

3.3. Performance evaluation of treated aging paper

To evaluate the performance of the treated aging paper with the stable nano MgO organic colloid, the treated papers samples were subjected to artificial accelerated aging for 3 days. The evaluation results in Table 1 indicated that the treated aging paper samples with ACMMHI presented the excellent deacidification, enhancement and anti-aging performance. First of all, the initial pH value of the treated aging paper samples with ACMMHI increased up to 8.30 from 4.70 and its alkaline reserve was 1.00% ($CaCO_3$ equivalent). After artificial accelerated aging for 3 days, the treated aging paper samples still presented the suitable pH value (7.38) and sufficient alkali reserves (0.90%, $CaCO_3$ equivalent), while the untreated paper samples further acidified (pH = 4.12). Moreover, comparing with the untreated aging paper samples, the initial tensile index and tear index of the treated aging paper samples with ACMMHI increased by 40.78% and 27.28%, respectively, which may be due to the enhancement of nano MgO and the cross-linking of $AKD_{0.024}$-g-$CMCC_{0.223}$ with paper fibers through electrostatic interaction. The great mechanical properties of nano MgO are beneficial to improving the mechanical behavior of treated paper sample (Kumar and Reddy 2020; Lisuzzo et al. 2021).

Table 1
The evaluation results of treated and untreated aging paper

Paper samples	pH Value	Alkaline reserve (%, $CaCO_3$ eq.)	ΔE	Tensile index (Nm/g)	Tear index ($mN·m^2/g$)	DP
UT	4.70 ± 0.06	-	-	20.92 ± 2.40	2.22 ± 0.12	324.49 ± 2.06
UT-Aging 3d	4.12 ± 0.08	-	4.62	16.84 ± 2.20 (-19.50%)	1.54 ± 0.10 (-30.64%)	205.93 ± 1.63
ACMMHI	8.30 ± 0.05	1.00	0.46	29.45 ± 3.40 (40.78%)	2.83 ± 0.25 (27.28%)	312.05 ± 1.85
ACMMHI-Aging 3d	7.38 ± 0.06	0.90	0.85	26.56 ± 2.00 (26.96%)	2.33 ± 0.17 (4.90%)	262.92 ± 2.24

Note: $\triangle E$ and the change in mechanical strength were calculated based on the untreated sample.

It can be further verified by the SEM-EDS in Fig. 6. The original mapping images were presented in Fig. S5. Compared with the untreated paper (Fig. 6a, 6c&6e), the SEM image of the treated paper with ACMMHI (Fig. 6b) clearly revealed the size of nano MgO (about 200 nm) evenly deposited on its surface. Furthermore, the mapping images (Fig. 6d) clearly presented more magnesium (Mg) element on the treated paper samples with ACMMHI. More element distribution of Nitrogen (N, 2.36%) and Mg (1.74%) of

treated paper samples with ACMMHI further supported the above conclusion. Thence, $AKD_{0.024}$-g-$CMCC_{0.223}$ containing positively charged quaternary ammonium groups (*DS* = 0.223) could form the electrostatic interaction with negatively charged hydroxyl groups of paper fiber to strengthen paper (Ren et al. 2018; He et al. 2019; Liu et al. 2020). After artificial accelerated aging for 3 days, the treated aging paper still remained higher tensile index (26.56 Nm/g), tear index (2.33 mN·m^2/g) and *DP* value (262.92) than the untreated aging paper (16.84 Nm/g, 1.54 mN·m^2/g, 205.93, respectively), which was attributed to the sufficient alkali reserves, inhibiting further acidification and degradation of aging paper.

Meanwhile, the treated aging paper samples with ACMMHI also presented the low ΔE (0.46). Although after accelerated aging for 3 days, the ΔE was still smaller (0.85) compared with the control (4.62), which is beneficial to reducing the yellowing of paper during the aging process. Furthermore, the photographs in Fig. S5 of the aging paper before and after treatment presented that the treatment of ACMMHI had no significantly influence in the appearance and clarity of writing. Additionally, as shown in Fig. S6, the static WCA of treated paper samples with ACMMHI reached 83^o comparing with the untreated aging book paper (the static WCA = 33^o), which may be due to the interaction between the long-chain alkanes of $AKD_{0.024}$-g-$CMCC_{0.223}$ and nano MgO deposited on the surface of treated paper samples. The suitable water resistance could prevent the treated paper pages from sticking during batch deacidification and reinforcement.

Conclusion

In summary, an amphiphilic cellulose-based copolymer ($AKD_{0.024}$-g-$CMCC_{0.223}$) was used to disperse nano MgO in low-polar HMDO with the help of IPA. After optimization, 0.50 wt.% of $AKD_{0.024}$-g-$CMCC_{0.223}$ endowed the nano MgO organic colloid with an excellent dispersion stability, small average particle size (200 nm) and low viscosity (2.26 mPa·s), which is beneficial for batch deacidification and reinforcement of aging paper. After evaluation, the treated aging paper with ACMMHI presented the excellent deacidification, enhancement and anti-aging performance. Improvement of paper mechanical performance was mainly owing to the cross-linking between $AKD_{0.024}$-g-$CMCC_{0.223}$ and paper fibers through electrostatic interaction. Meanwhile, the great mechanical properties of nano MgO deposited in the networks of paper fibers was also important factor to improve the mechanical performance of treated paper. Moreover, the sufficient alkali reserve promoted the anti-aging performance by inhabiting further acidification and degradation of aging paper. Additionally, the mild pH value was also beneficial to reducing the yellowing of aging paper. Therefore, this novel and efficient protection strategy based on $AKD_{0.024}$-g-$CMCC_{0.223}$ stabilizing nano MgO in the low-polar mixed solvent of HMDO and IPA will have great application prospects for the protection of aging paper.

Declarations

Acknowledgments

This work was financially supported by National Natural Science Foundation of China (22178128), and Science and Technology Plan Special Project of Guangzhou, China (No. GZDD201808).

The authors declare that they have no conflict of interest.

Supporting Information

The chemical structures and reaction process of CMCC and AKD-g-CMCC (Fig. S1), response peaks and the molecular weight distribution of AKD (Fig. S2), original solid state ^{13}C-NMR spectrum of (a) MCC, (b) CMCC, (c~e) three kinds of AKD-g-CMCC, and (f) AKD (Fig. S3), viscosity of nano-MgO organic colloid containing 0.1~0.7 wt.% $AKD_{0.024}$-g-$CMCC_{0.223}$ (Fig. S4), original mapping images of untreated aging paper sample and treated aging paper sample with ACMMHI (Fig. S5), photographs and static WCA of the naturally aged-book papers before and after treatment with ACMMHI (Fig. S6), the corresponding integral of various types of C on the solid-state ^{13}C NMR spectra of MCC, CMCC, and three kinds of AKD-g-CMCC polymers (Table S1), and the $[\eta]$, M_r and ratio of grafted groups of $AKD_{0.009}$-g-$CMCC_{0.277}$, $AKD_{0.027}$-g-$CMCC_{0.253}$, and $AKD_{0.024}$-g-$CMCC_{0.223}$ (Table S2) were mentioned in this manuscript.

References

1. Amornkitbamrung L, Mohan T, Hribernik S, Reichel V, Faivre D, Gregorova A, Engel P, Kargl R, Ribitsch V (2015) Polysaccharide stabilized nanoparticles for deacidification and strengthening of paper. RSC Adv 42: 32950-32961.
2. Amornkitbamrung L, Marnul M C, Palani T, Hribernik S, Kovalcik A, Kargl R, Stana-Kleinschek K, Mohan T (2018) Strengthening of paper by treatment with a suspension of alkaline nanoparticles stabilized by trimethylsilyl cellulose. Nano-Structures & Nano-Objects 16: 363-370.
3. Amornkitbamrung L, Bračič D, Bračič M, Hribernik S, Malešič J, Hirn U, Mohan T (2020) Comparison of trimethylsilyl cellulose-stabilized carbonate and hydroxide nanoparticles for deacidification and strengthening of cellulose-based cultural heritage. ACS omega 45: 29243-29256.
4. Area M C, Ceradame H (2011) Paper aging and degradation: recent findings and research methods. Bioresources 6: 5307-5337.
5. Baglioni P, Berti D, Bonini M, Carretti E, Dei L, Fratini E, Giorgi R (2014) Micelle, microemulsions, and gels for the conservation of cultural heritage. Adv Colloid Interface Sci 205: 361-371.
6. Baglioni P, Chelazzi D, Giorgi R (2015) Nanotechnologies in the conservation of cultural heritage: a compendium of materials and techniques. Springer.
7. Baty J W, Maitland C L, Minter W, Hubbe M A, Jordan-Mowery S K (2010) Deacidification for the conservation and preservation of paper-based works: A review. Bioresources 5: 1955-2023.
8. Cappitelli F, Pasquariello G, Tarsitani G, Sorlini C (2010) Scripta manent? Assessing microbial risk to aging paper. Trends Microbiol 18: 538-542.

9. Carter H A (1996a) The chemistry of paper preservation: Part 1. the aging of paper and conservation techniques. J Chem Educ 73: 417.
10. Carter H A (1996b) The chemistry of paper preservation: Part 2. The yellowing of paper and conservation bleaching. J Chem Educ 73: 1068.
11. Chaker A, Boufi S (2015) Cationic nanofibrillar cellulose with high antibacterial properties. Carbohydr polym 131: 224-232.
12. Cheradame H, Ipert S, Rousset E (2003) Mass deacidification of paper and books. I: Study of the limitations of the gas phase processes. Restaurator 24: 227-239.
13. Chung J, Lee J, Choe E (2004) Oxidative stability of soybean and sesame oil mixture during frying of flour dough. J Food Sci 69: 574-578.
14. Conte A M, Pulci O, Knapik A, Bagniuk J, Del Sole R, Lojewska J, Missori M (2012) Role of cellulose oxidation in the yellowing of ancient paper. Phys Rev Lett 108: 158301.
15. Esmaeili A R, Mir N, Mohammadi R (2020) A facile, fast, and low-cost method for fabrication of micro/nano-textured superhydrophobic surfaces. J Colloid Interface Sci 573: 317-327.
16. Ferrandin-Schoffel N, Haouas M, Martineau-Corcos C, Fichet O, Dupont A L (2020) Modeling the reactivity of aged paper with aminoalkylalkoxysilanes as strengthening and deacidification agents. ACS Appl Polym Mater 2: 1943-1953.
17. Giorgi R, Baglioni M, Berti D, Baglioni P (2010) New methodologies for the conservation of cultural heritage: micellar solutions, microemulsions, and hydroxide nanoparticles. Acc Chem Res 43: 695-704.
18. Harini K, Ramya K, Sukumar M (2018) Extraction of nano cellulose fibers from the banana peel and bract for production of acetyl and lauroyl cellulose. Carbohydr Polym 201: 329-339.
19. Hubbe M A, Henniges U, Potthast A, Ahn K, Smith R D (2018) Nonaqueous solution deacidification treatments to prolong the storage life of acidic books: A review of mechanistic and process aspects. Bioresources 13: 7096-7136.
20. He B, Lin Q, Chang M, Liu C, Fan H, Ren J (2019) A new and highly efficient conservation treatment for deacidification and strengthening of aging paper by in-situ quaternization. Carbohydr Polym 209: 250-257.
21. Hubbe M A, Smith R D, Zou X, Katuscak S, Potthast A, Ahn K (2017) Deacidification of acidic books and paper by means of non-aqueous dispersions of alkaline particles: A review focusing on completeness of the reaction. Bioresources 12: 4410-4477.
22. Isca C, D'Avorgna S, Graiff C, Montanari M, Ugozzoli F, Predieri G (2016) Paper preservation with polyamidoamines: a preliminary study. Cellulose 23: 1415-1432.
23. Isca C, Di Maggio R, Collado N P, Predieri G, Lottici P P (2019) The use of polyamidoamines for the conservation of iron-gall inked paper Cellulose 26: 1277-1296.
24. Jeong M J, Bogolitsyna A, Jo B M, Kang K Y, Rosenau T, Potthast A (2014) Deterioration of ancient Korean paper (Hanji) treated with beeswax: A mechanistic study. Carbohydr Polym 101: 1249-1254.

25. Jeon S J, Yu J E, Han Y W, Suh I S, Moon D K (2019) Structural optimization in the same polymer backbones for efficient polymer solar cells: Relationship between steric hindrance and molecular weight. J Ind Eng Chem 71: 137-149.
26. Jiang F, Yang Y, Weng J, Zhang X (2016) Layer-by-layer self-assembly for reinforcement of aged papers. Ind Eng Chem Res 55: 10544-10554.
27. Jiazhen L, Jingxuan W (2010) Main factors affecting the preservation of Chinese paper documents: A review and recommendations. IFLA J 36: 227-234.
28. Jia Z, Yang C, Zhao F, Chao X, Li Y, Xing H (2020) One-step reinforcement and deacidification of paper documents: Application of Lewis base—Chitosan nanoparticle coatings and analytical characterization. Coatings 10: 1226.
29. Kono H (2017) Cationic flocculants derived from native cellulose: Preparation, biodegradability, and removal of dyes in aqueous solution. Resource-Efficient Technol 3: 55-63.
30. Kumar K S, REDDY A C (2020) Experimental investigation on mechanical and tribological properties of MgO/ABS polymer composites. Int J Mech Prod Eng Res Dev 10: 449-458.
31. Lama E, Veneranda M, Prieto-Taboada N, Hernando F L, Laso M R, Madariaga J M (2020) A first evaluation of the usefulness of Kudzu starch in cultural heritage restoration. Sci Rep 10: 1-10.
32. Li M C, Mei C, Xu X, Lee S, Wu Q (2016) Cationic surface modification of cellulose nanocrystals: Toward tailoring dispersion and interface in carboxymethyl cellulose films. Polymer 107: 200-210.
33. Li Y, Li Z, Shen G, Zhan Y (2019) Paper conservation with an aqueous NaOH/urea cellulose solution. Cellulose 26: 4589-4599.
34. Lisuzzo L, Cavallaro G, Milioto S, Lazzara G (2021) Halloysite nanotubes filled with MgO for paper reinforcement and deacidification. Appl Clay Sci 213: 106231.
35. Liu C F, Xu F, Sun J X, Ren J L, Curling S, Sun R C, Baird M S (2006) Physicochemical characterization of cellulose from perennial ryegrass leaves (Lolium perenne). Carbohydr Res 341: 2677-2687.
36. Liu X, Yang K, Chang M, Wang X, Ren J (2020) Fabrication of cellulose nanocrystal reinforced nanocomposite hydrogel with self-healing properties. Carbohydr Polym 240: 116289.
37. Ma X, Tian S, Li X, Fan H, Fu S (2021) Combined polyhexamethylene guanidine and nanocellulose for the conservation and enhancement of ancient paper. Cellulose 28: 8027-8042.
38. Narouz M R, Li C H, Nazemi A, Crudden C M (2017) Amphiphilic N-heterocyclic carbene-stabilized gold nanoparticles and their self-assembly in polar solvents. Langmuir 33: 14211-14219.
39. Norris D H, Gutierrez J J (2017) Preventing destruction: preserving our irreplaceable photographic peritage. Am Art 31: 18-23.
40. Odabas N, Amer H, Bacher M, Henniges U, Potthast A, Rosenau T (2016) Properties of cellulosic material after cationization in different solvents. ACS Sustain Chem Eng 4: 2295-2301.
41. Odabas N, Amer H, Henniges U, Potthast A, Rosenau T (2017) A comparison of methods to quantify cationization of cellulosic pulps. J Wood Chem Technol 37: 136-147.

42. Palladino N, Hacke M, Poggi G, Nechyporchuk O, Kolman K, Xu Q, Bordes R (2020) Nanomaterials for combined stabilisation and deacidification of cellulosic materials—the case of iron-tannate dyed cotton. Nanomaterials 10: 900.
43. Pereira-Pardo L, Korenberg C (2018) The use of erbium lasers for the conservation of cultural heritage. A review. J Cult Herit 31: 236-247.
44. Potthast A, Ahn K (2017) Critical evaluation of approaches toward mass deacidification of paper by dispersed particles. Cellulose 24: 323-332.
45. Ran Q, Somasundaran P, Miao C, Liu J, Wu S, Shen J (2009) Effect of the length of the side chains of comb-like copolymer dispersants on dispersion and rheological properties of concentrated cement suspensions. J Colloid Interface Sci 336: 624-633.
46. Ren J, Dai Q, Zhong H, Liu X, Meng L, Wang X, Xin F (2018) Quaternized xylan/cellulose nanocrystal reinforced magnetic hydrogels with high strength. Cellulose 25: 4537-4549.
47. Reynaert S, Moldenaers P, Vermant J (2006) Control over colloidal aggregation in monolayers of latex particles at the oil– water interface. Langmuir 22: 4936-4945.
48. Santos S M, Carbajo J M, Quintana E, Ibarra D, Gomez N, Ladero M, Villar J C (2015) Characterization of purified bacterial cellulose focused on its use on paper restoration. Carbohydr Polym 116: 173-181.
49. Schwanninger M J C R, Rodrigues J C, Pereira H, Hinterstoisser B (2004) Effects of short-time vibratory ball milling on the shape of FT-IR spectra of wood and cellulose. Vib Spectrosc 36: 23-40.
50. Shinoda R, Saito T, Okita Y, Isogai A (2012) Relationship between length and degree of polymerization of TEMPO-oxidized cellulose nanofibrils. Biomacromolecules 13: 842-849.
51. Sirviö J, Honka A, Liimatainen H, Niinimäki J, & Hormi O (2011) Synthesis of highly cationic water-soluble cellulose derivative and its potential as novel biopolymeric flocculation agent. Carbohydr Polym 86: 266-270.
52. Shukla G, Shahi V K (2018) Poly (arylene ether ketone) copolymer grafted with amine groups containing a long alkyl chain by chloroacetylation for improved alkaline stability and conductivity of anion exchange membrane. ACS Appl Energy Mater 1: 1175-1182.
53. Song X, Chen F, Liu F (2012) Preparation and characterization of alkyl ketene dimer (AKD) modified cellulose composite membrane. Carbohydr Polym 88: 417-421.
54. Tyagi P, Hubbe M A, Lucia L, Pal L (2018) High performance nanocellulose-based composite coatings for oil and grease resistance. Cellulose 25: 3377-3391.
55. Wang T, Okejiri F, Qiao Z A, Dai S (2020) Tailoring polymer colloids derived porous carbon spheres based on specific chemical reactions. Adv Mater 32: 2002475.
56. Wilson A (2012) Library policy for preservation and conservation in the European Community. KG Saur.
57. Xu Q, Poggi G, Resta C, Baglioni M, Baglioni P (2020) Grafted nanocellulose and alkaline nanoparticles for the strengthening and deacidification of cellulosic artworks. J Colloid Interface Sci

576: 147-157.
58. Xu J, Zhang T, Jiang Y, Yang D, Qiu F, Chen Q, Yu Z (2020) Preparation of self-healing acrylic copolymer composite coatings for application in protection of paper cultural relics. Polym Eng Sci 60: 288-296.
59. Yang L, Lu S, Li J, Zhang F, Cha R (2016) Nanocrystalline cellulose-dispersed AKD emulsion for enhancing the mechanical and multiple barrier properties of surface-sized paper. Carbohydr Polym 136: 1035-1040.
60. Yan Y, Amer H, Rosenau T, Zollfrank C, Dörrstein J, Jobst C, Li J (2016) Dry, hydrophobic microfibrillated cellulose powder obtained in a simple procedure using alkyl ketene dimer. Cellulose 23: 1189-1197.
61. Yi C, Yang Y, Liu B, He J, Nie Z (2020) Polymer-guided assembly of inorganic nanoparticles. Chem Soc Rev 49: 465-508.
62. Zervos S, Alexopoulou I (2015) Paper conservation methods: a literature review. Cellulose 22: 2859-2897.

Figures

Figure 1

Schematic diagram of the preparation and application of AKD-g-CMCC.

Figure 2

(a) FT-IR spectra of MCC, CMCC, AKD, and AKD-g-CMCC polymers. (b) Partial enlarged views of the FT-IR spectra of MCC, CMCC at 1500~900 cm^{-1}.

Figure 3

Solid state ^{13}C-NMR spectrum of (a) MCC, (b) CMCC, (c~e) three kinds of AKD-g-CMCC, and (f) AKD.

Figure 4

(a) Transmittance of nano MgO organic colloid containing different AKD-g-CMCC after standing 0, 12, and 24 hours. (b) Transmittance of nano MgO organic colloid containing 0.1, 0.3, 0.5, and 0.7 wt.%

$AKD_{0.024}$-g-$CMCC_{0.223}$ after standing 0 and 24 hours. (c) Transmittance of different dispersion systems after standing 0~12 hours. (d) Particle size distribution of different nano MgO organic colloids.

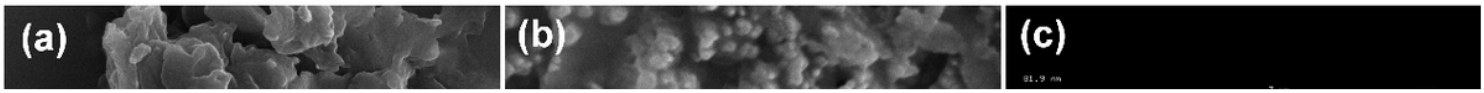

Figure 5

SEM images of 0.5 wt.% $AKD_{0.024}$-g-$CMCC_{0.223}$/HMDO/IPA (5:5) (a) and 0.5 wt.% $AKD_{0.024}$-g-$CMCC_{0.223}$/MgO/HMDO/IPA (5:5) (b). (c) AFM image of 0.5 wt.% $AKD_{0.024}$-g-$CMCC_{0.223}$/MgO/HMDO/IPA (5:5).

Figure 6

(a) SEM images of the untreated aging paper sample (UT). (b) SEM images of the treated aging paper sample with ACMMHI. (c) Mapping of UT and (d) Mapping of ACMMHI. (e) Element distribution of the treated aging paper sample with UT and ACMMHI.

Supplementary Files

This is a list of supplementary files associated with this preprint. Click to download.

- Graphicalabstract.png
- surportinginformation2022.02.09.docx